Journal of Biomolecular NMR, **11:** 165–183, 1998.
KLUWER/ESCOM

Dynamics of β-CH and β-CH_2 groups of amino acid side chains in proteins

Jan Engelke and Heinz Rüterjans*
Institut für Biophysikalische Chemie der Johann-Wolfgang Goethe Universität Frankfurt am Main, Biozentrum N230, Marie-Curie Strasse 9, D-60439 Frankfurt am Main, Germany

Received 16 September 1997; Accepted 30 September 1997

Key words: ^{13}C relaxation times, protein dynamics, ribonuclease T1, side chain motion

Abstract

The dynamics of amino acid side chains of uniformly $^{13}C/^{15}N$-enriched ribonuclease T1 (RNase T1) have been investigated. Heteronuclear longitudinal relaxation rates, $^{1}H/^{13}C$ NOEs, and transverse cross-correlated cross-relaxation rates between the S_x and the $S_x I_z^1 I_z^2$ operators (SIIS cross relaxation) [Ernst and Ernst (1994) *J. Magn. Reson.*, **A110**, 202–213] have been determined in this study. New pulse sequences for measuring the longitudinal relaxation time and the heteronuclear NOE of aliphatic side chain carbon nuclei were developed using the CCONH type of magnetization transfer and $^{1}H^{N}$ detection. In addition, an improved pulse sequence for the determination of the SIIS cross relaxation is presented. For the analysis of the relaxation rates, the model of restricted rotational diffusion around the χ_1 dihedral angle has been applied [London and Avitabile (1978) *J. Am. Chem. Soc.*, **100**, 7159–7165]. These techniques were used in order to describe the side chain dynamics of the small globular protein RNase T1 (104 amino acids, MW about 11 kDa). Qualitative values of microdynamical parameters were obtained for 73 out of 85 amino acid side chains (glycine and alanine residues excepted) whereas more quantitative values were derived for 67 β-CH and β-CH_2 groups.

Introduction

Dynamic aspects of peptide and protein structures are increasingly recognized as being important for a description of their biological functions. As a consequence, considerable effort has been made to characterize protein and peptide side chain and backbone motions, mainly through fluorescence spectroscopy (Palmer et al., 1993), NMR relaxation (Kay et al., 1989; Clore et al., 1990a; Stone et al., 1992; Szyperski et al., 1993; Fushman et al., 1994; Habazettl et al., 1996), amide proton exchange studies (Loh et al., 1993), molecular dynamics simulations (Palmer and Case, 1992; Schmidt et al., 1993; Balasubramanian et al., 1994; Smith et al., 1995) and X-ray studies (Buck et al., 1995). ^{13}C NMR relaxation, in particular, is sensitive to probe motions of a broad range of time scales and can be used to describe the dynamics of various groups within a protein (Richarz et al., 1980; Henry et al., 1986; Nirmala and Wagner, 1988; Palmer et al., 1991; Nicholson et al., 1992; Daragan and Mayo, 1996).

For a quantitative study of side chain motions, a large number of degrees of freedom caused by various diffusion or jump processes around different axes of orientations have to be considered. Such an analysis seems to be very complex, in particular in the case of long side chains. Therefore as a first attempt, we would like to investigate the dynamics of the χ_1 dihedral angle, which connects a β-CH, -CH_2 or -CH_3 group to C^{α} of the corresponding amino acid. Frequently, the internal dynamics of this dihedral angle is analysed using motionally averaged ^{3}J coupling constants like $^{3}J_{H^{\alpha}H^{\beta 1}}$, $^{3}J_{H^{\alpha}H^{\beta 2}}$, vicinal carbon-proton, nitrogen-proton and carbon-carbon coupling constants (Karplus, 1959,1963; Bystrov, 1976). Starting with a small number of discrete conformations characterized by different χ_1 angles, the theoretical ^{3}J coupling constants are calculated using the Karplus relations (Mádi et al., 1990). Populations of individual staggered rotamer conformations are obtained by fitting the value

* To whom correspondence should be addressed.

of the calculated ^{3}J coupling constant to the experimental value. This analysis has already been carried out for most of the χ_1 dihedral angles of the side chains in ribonuclease T1 (RNase T1) (Karimi-Nejad et al., 1994). However, no information about the rate constants of transfer between the various rotameric states can be obtained from averaged J coupling constants. Therefore, in this paper, we try to describe the dynamics of the χ_1 angle using heteronuclear relaxation rates.

Two different types of relaxation rates were investigated: the heteronuclear longitudinal relaxation process described by the T_1 relaxation time together with the heteronuclear ^{1}H/^{13}C nuclear Overhauser effect (NOE) and the transverse heteronuclear cross-correlated cross-relaxation rate between the S_x single quantum and the $4S_xI_z^1I_z^2$ triple quantum operator in $^{13}CH_2$ groups (Ernst and Ernst, 1994). The longitudinal relaxation and the steady-state NOE of the C^β nucleus are dominated by the dipolar interaction(s) with its directly bound proton(s). Minor contributions stem from the anisotropy of the ^{13}C shielding tensor (CSA), from the dipolar-CSA cross correlation and from the cross correlation between the dipolar interactions of CH_2 groups. In the analysis, it will be shown that neglecting the latter three interactions will not lead to major problems in the interpretation of the results in terms of molecular motion. The dipolar carbon-proton interaction is modulated by the overall molecular rotational tumbling and by torsional motions. The latter is relaxation-active only for motions with a torsional time constant $\tau_{\chi_1} \leq \tau_C$, τ_C being the overall correlation time of the protein. Processes with $\tau_{\chi_1} \gg \tau_C$ do not affect the longitudinal relaxation or the NOE and therefore cannot be analysed using this approach. The second technique is called SIIS cross relaxation and can be used to analyse the dynamics of CH_2 groups. The basic process depends on the motional cross correlation of two CH dipolar interactions. In a particular range of intermolecular motional correlation times, it allows a distinction of restricted and unrestricted intramolecular motion.

Theoretical aspects

Choice of model of motion

The problem of adequately describing protein side chain dynamics by NMR relaxation normally is connected with limited experimental data and with the choice of appropriate model assumptions. Models currently used for the analysis of NMR relaxation data include those which describe anisotropic unrestricted diffusion, multiple rotations, restricted diffusion (see, for example, a review by London (1980) and wobbling-in-a-cone motions (Lipari and Szabo, 1980,1981). Various model-free approaches (Lipari and Szabo, 1982a,b; Clore et al., 1990a,b) for obtaining information about overall rotational correlation times and characteristics of restricted motions in terms of order parameters are also available. With limited experimental data, it is often difficult to decide which model is best, and the simplest model that can describe the available experimental parameters is used in most cases. For example, detailed investigations were carried out for the dynamics of the phenylalanine side chains in antamanide, but even for this small peptide a distinction between a diffusion motion and a jump motion was difficult to make (Ernst, 1993). Hence, a decision about the type of motion will not be made but rather the amplitude and the time scale of the motion using a fixed model of motion should be quantitatively determined. To date, the model-free approach has been used most often. This may be reasonable for investigations of the protein backbone, but it fails in more detailed descriptions of protein side chain dynamics. In order to cover a wide range of amplitudes and time scales of motions around the χ_1 dihedral angle, the rotational restricted diffusion model has been chosen for the interpretation of the relaxation data (London and Avitabile, 1978). In this model, the $^{13}C^\beta$-$^1H^\beta$ vector moves around χ_1 with an amplitude in the range $-\gamma_{max} \leq \gamma \leq \gamma_{max}$. In cases where γ_{max} extends $60\,^\circ$, the dynamics may be adequately described with jump models. However, a distinction between different types of models is not possible due to the limited number of available experimental data.

T_1 relaxation time and steady-state NOE

In order to study the motion around the χ_1 dihedral angle, the T_1 relaxation time and the heteronuclear ^{1}H/^{13}C NOE of the C^β nucleus were used. The inclusion of the transverse relaxation time in the analysis might also be conceivable. However, for measuring the T_2 relaxation time a pulse sequence has to be available which effectively suppresses the scalar ^{13}C-^{13}C coupling during the T_2 evolution period. While such a pulse sequence has already been developed for the $^{13}C^\alpha$ nucleus (Yamazaki et al., 1994; Engelke and Rüterjans, 1995), its application to side chain carbon nuclei fails in most cases due to the small difference in the chemical shift of adjacent ^{13}C nuclei.

In the analysis of the longitudinal relaxation rates of the $^{13}C^{\beta}$ nucleus, several relaxation contributions have to be considered. In case of an isolated SI spin system, the $^{13}C^{\beta}$ NMR relaxation is caused by the dipole-dipole interaction with its bound proton, by magnetic shielding due to the chemical shift anisotropy (CSA) and by a cross correlation between these two interactions. In general, equations for the initial relaxation rates of the left (ρ^-) and right line (ρ^+) of the ^{13}CH doublet are given by (Goldman, 1984; Bull, 1992)

$$\rho^+ = \rho_{CH} + \rho_{CSA} + \rho_{CHA} \quad (1a)$$

$$\rho^- = \rho_{CH} + \rho_{CSA} - \rho_{CHA} \quad (1b)$$

where

$$\rho_{CH} = \frac{1}{20}\frac{\gamma_C^2\,\gamma_H^2}{r_{CH}^6}\left(\frac{h}{2\pi}\right)^2 \left(\frac{\mu_0}{4\pi}\right)^2 J_{CH}^*(\omega) \quad (2a)$$

$$\rho_{CSA} = \frac{1}{15}\Delta\delta^2\,\omega_C^2\,J_{CSA}(\omega_C) \quad (2b)$$

$$\rho_{CHA} = \frac{2}{5}\frac{\gamma_C\,\gamma_H\,\Delta\delta\,\omega_C}{r_{CH}^3}\left(\frac{h}{2\pi}\right) \left(\frac{\mu_0}{4\pi}\right) J_{CHA}(\omega_C) \quad (2c)$$

h is Planck's constant (6.626×10^{-34} Js), r_{CH} is the internuclear distance between the carbon and its bound hydrogen (1.10 Å), $\Delta\delta$ is the chemical shift anisotropy constant (50 ppm) (Ye et al., 1993) and γ_C and γ_H are the gyromagnetic ratios for carbon ($6.728 \cdot 10^7$ T^{-1} s^{-1}) and hydrogen nuclei (2.6752×10^8 $T^{-1}s^{-1}$), respectively. The spectral densities are defined by

$$J_{CH}^*(\omega) = J_{CH}(\omega_H - \omega_C) + 3J_{CH}(\omega_C) + 6J_{CH}(\omega_H + \omega_C) \quad (3)$$

where ω_C and ω_H are the ^{1}H and ^{13}C resonance frequencies, respectively, and $J_{CH}(\omega)$ is represented by

$$J_{CH}(\omega) = 4\pi \int_{-\infty}^{\infty} \langle Y_{20}(\Omega_{CH}(t)) Y_{20}(\Omega_{CH}(0))\rangle e^{-i\omega t}\,dt \quad (4)$$

In this spectral density function, Y_{20} is the second-rank spherical harmonic and Ω_{CH} are the CH bond spherical polar angles (θ and ϕ) in the laboratory frame. $J_{CSA}(\omega_C)$ is the carbon CSA autocorrelation spectral density and $J_{CHA}(\omega_C)$ defines the spectral density for the cross correlation between a carbon-hydrogen dipolar interaction and the carbon CSA tensor (Hartzell et al., 1989). In order to estimate the parts of the individual relaxation contributions, an isotropic reorientation of the molecule with an overall tumbling correlation time of 5 ns is assumed. Using a carbon resonance frequency of 125 MHz, the relaxation rates yield at $\rho_{CH} = 2.21\ s^{-1}$, $\rho_{CSA} = 0.0626\ s^{-1}$ and $\rho_{CHA} = -0.467\ s^{-1}$. The contribution of the CSA term amounts to about 3% and can therefore be neglected. Nevertheless, the influence of dipolar-heteronuclear CSA cross correlation is significant and can affect measurements of T_1 and NOE. Fortunately, this contribution can be eliminated from T_1 measurements by continuous inversion of the proton resonance during the relaxation period so that only the dipolar carbon-proton interaction has to be considered for β-CH groups (Boyd et al., 1990; Kay et al., 1992).

For an isolated CH_2 spin system, equations for the initial relaxation rates of inner (ρ_I) and left (ρ_O^-) and right (ρ_O^+) outer lines of the $^{13}CH_2$ multiplet can be expressed as (Daragan et al., 1993; Daragan and Mayo, 1993a)

$$\rho_I = \rho_{CH} + \rho_{CSA} - \rho_{HCH} \quad (5a)$$

$$\rho_O^{\pm} = \rho_{CH} + \rho_{CSA} + \rho_{HCH} \pm \rho_{CHA} \quad (5b)$$

where

$$\rho_{CH} = \frac{2}{20}\frac{\gamma_C^2\,\gamma_H^2}{r_{CH}^6}\left(\frac{h}{2\pi}\right)^2\left(\frac{\mu_0}{4\pi}\right)^2 J_{CH}^*(\omega) \quad (6a)$$

$$\rho_{HCH} = \frac{3}{10}\frac{\gamma_C^2\,\gamma_H^2}{r_{CH}^6}\left(\frac{h}{2\pi}\right)^2\left(\frac{\mu_0}{4\pi}\right)^2 J_{HCH}(\omega) \quad (6b)$$

The function $J_{HCH}(\omega)$ is the dipolar cross-correlation function:

$$J_{HCH}(\omega) = 4\pi \int_{-\infty}^{\infty} \langle Y_{20}(\Omega_{CH^1}(t)) Y_{20}(\Omega_{CH^2}(0))\rangle e^{-i\omega t}\,dt \quad (7)$$

where CH^1 and CH^2 are the two methylene CH vectors. For the isotropic reorientation of the molecule, the spectral density function is given by

$$J_{HCH}(\omega_C) = P_2[\cos(\vartheta_{HCH})]\frac{2\tau_C}{1+(\omega_C\tau_C)^2} = -\frac{1}{3}\frac{2\tau_C}{1+(\omega_C\tau_C)^2} \quad (8)$$

where the last term is valid for an ideal tetrahedral geometry ($\vartheta_{HCH} = 109.4710°$). For $\tau_C = 5$ ns and $\omega_C = 2\pi \times 125$ MHz, ρ_{HCH} amounts to $-1.31\ s^{-1}$. Hence, even under proton saturation the cross correlation between the dipolar interactions leads to a double-exponential decay of the longitudinal magnetization. Zhu et al. (1995) studied the magnitude of the error when fitting the longitudinal magnetization decay to a single exponential function. They applied several different methods of data reduction and found, all in all, that the errors in T_1 and the NOE are less than 6% and 4%, respectively. Therefore, neglecting dipolar cross correlation in ^{13}C T_1 and NOE measurements in SI_2 systems does not lead to major problems in the interpretation of the results in terms of molecular motion. Thus, for isolated β-CH and β-CH_2 groups only the dipolar interaction(s) with its directly bound proton(s) have to be considered.

In a uniformly ^{13}C-enriched protein, the $^{13}C^\beta$ nucleus is surrounded by several other ^{13}C nuclei. Therefore, besides the n directly bound protons the homonuclear ^{13}C-^{13}C dipolar interactions contribute to its relaxation. The equation describing the relaxation of a $^{13}C^\beta$spin in a homonuclear environment is given by

$$\frac{d}{dt}C_z^\beta = -R_{C^\beta}(\langle C_z^\beta\rangle - C_{eq}^\beta) - \sigma_{C^\beta C^\alpha}(\langle C_z^\alpha\rangle - C_{eq}^\alpha) - \sigma_{C^\beta C^\gamma}(\langle C_z^\gamma\rangle - C_{eq}^\gamma) \quad (9)$$

where $R_{C^\beta} = n\,\rho_{C^\beta H^\beta} + \rho_{C^\beta C^\alpha} + m\,\rho_{C^\beta C^\gamma}$. n is the number of H^β protons, m is the number of γ-carbons directly bound to the $^{13}C^\beta$ nucleus and ρ_{CC} is the homonuclear longitudinal relaxation rate between two carbon nuclei:

$$\rho_{CC} = \frac{1}{20}\frac{\gamma_C^4}{r_{CC}^6}\left(\frac{h}{2\pi}\right)^2\left(\frac{\mu_0}{4\pi}\right)^2(J_{CC}(0) + 3J_{CC}(\omega_C) + 6J_{CC}(2\omega_C)) \quad (10)$$

It was shown previously (Engelke and Rüterjans, 1995) that when using an experiment in which the chemical shift is recorded prior to the relaxation period T, cross peaks at the frequency (Ω_{C^β}, Ω_{H^N}), (Ω_{C^α}, Ω_{H^N}) and (Ω_{C^γ}, Ω_{H^N}) will appear in the 2D spectrum. Since the latter two terms are proportional to $\sigma_{C^\beta C^\alpha}$ and $\sigma_{C^\beta C^\gamma}$, only very weak cross peaks will be observed. In proteins these cross peaks were not seen. The contribution of the cross-relaxation rates $\sigma_{C^\beta C^\alpha}$ and $\sigma_{C^\beta C^\gamma}$ to the first term is of second order such that an error of no more than 2–4% in the measured values of R_{C^β} should be obtained when fitting the experimental data to a single exponential. For the heteronuclear NOE, an additional contribution due to cross relaxation can be expected. Following the detailed analysis of the relaxation of the $^{13}C^\alpha$ nucleus in the absence and presence of a directly bound β-methyl group with normally large NOE values, it was shown that the contribution of the cross relaxation $\sigma_{C^\beta C^\alpha}$ and $\sigma_{C^\beta C^\gamma}$ does not lead to errors larger than 5% (Engelke and Rüterjans, 1995). The correlation between the longitudinal relaxation rates and the spectral densities is approximately given by

$$\frac{1}{T_1} = n\,\rho_{C^\beta H^\beta} + \rho_{C^\beta C^\alpha} + m\,\rho_{C^\beta C^\gamma} \quad (11a)$$

$$NOE = 1 + \frac{\gamma_H}{\gamma_C}\frac{n\,\sigma_{C^\beta H^\beta}}{n\,\rho_{C^\beta H^\beta} + \rho_{C^\beta C^\alpha} + m\,\rho_{C^\beta C^\gamma}} \quad (11b)$$

In order to extract microdynamical parameters from the relaxation rates, a specific model for the molecular motion has to be chosen. Assuming that the reorientation of the protein is isotropic and that the side chain motion almost exclusively originates from rotations around the C-C bond, the general expression of the autocorrelation function for the $^{13}C^\beta$-$^1H^\beta$ vector is given by (Wittebort and Szabo, 1978)

$$C(t) = \frac{1}{4\pi}e^{-6Dt}\sum_{m_1=-2}^{2}\langle e^{im_1\chi_1(t)}e^{-im_1\chi_1(0)}\rangle\, r_{0,m_1}^2(\beta_2)r_{0,m_1}^2(\beta_2) \quad (12)$$

where $r_{0,m_1}^2(\beta_2)$ are the elements of the Wigner rotation matrix of second order and $D = 1/6\tau_C$. The angle β_2 amounts to 109.5° for an ideal tetrahedral geometry. For a restricted diffusion motion around the χ_1 dihedral angle in the range between $\pm\gamma_{max}$, the correlation function is given by (London and Avitabile, 1978)

$$C(t) = \frac{1}{4\pi} e^{-6Dt} \sum_{l=-2}^{2} \sum_{j=0}^{\infty} a_l (E_{l,j}(\gamma_{\max}))^2 \; e^{-D_1 j^2 \pi^2 t/(4\gamma_{\max})} \quad (13)$$

where $D_1 = 1/\tau_i$. The spectral density function is obtained by Fourier transformation:

$$J(\omega) = J_{CH}(\omega) = J_{HCH}(\omega) = \sum_{l=-2}^{2} \sum_{j=0}^{\infty} a_l (E_{l,j}(\gamma_{\max}))^2 \frac{2\tau_{cj}}{1 + (\omega\tau_{cj})^2} \quad (14)$$

with $E_{l,j}(\gamma_{\max})$ defined by

$$E_{l,j}(\gamma_{\max}) = \begin{cases} \frac{\sin(m\gamma_{\max})}{m\gamma_{\max}} & \text{for } j = 0 \\ \frac{1}{\sqrt{2}} \left(\frac{\sin(m\gamma_{\max} - j\frac{\pi}{2})}{m\gamma_{\max} - j\frac{\pi}{2}} + (-1)^j \frac{\sin(m\gamma_{\max} + j\frac{\pi}{2})}{m\gamma_{\max} + j\frac{\pi}{2}} \right) & \text{for } j \neq 0 \end{cases} \quad (15)$$

and

$$\tau_{cj} = \frac{4\gamma_{\max}}{24D\gamma_{\max}^2 + D_1 j^2 \pi^2} \quad (16)$$

The constants are given by $a_{\pm 2} = 0.2961$, $a_{\pm 1} = 0.1486$ and $a_0 = 0.1107$. Since it is assumed that the internal motion is caused by a rotation around the $^{13}C^{\alpha}$-$^{13}C^{\beta}$ bond, the spectral density function for the contribution $\rho_{C^{\alpha}C^{\beta}}$ is that of a rigid rotator. However, the motion of the $^{13}C^{\beta}$-$^{13}C^{\gamma}$ bond is identical to that of the $^{13}C^{\beta}$-$^{1}H^{\beta}$ bond and therefore the expression for the spectral density function of $\rho_{C^{\beta}C^{\gamma}}$ is given by Equation 14.

In Figure 1 the heteronuclear NOE of the $^{13}C^{\beta}$ nucleus is shown in dependence of the amplitude $\gamma_{\max}$ and the internal correlation time τ_i. For a strongly restricted motion a small heteronuclear NOE is expected, which is independent of the internal correlation time. Motions with larger amplitudes should lead to larger NOE values. From this dependence, a certain limit for the amplitude of motion can be derived from the NOE value. For example, a NOE value of 1.8 can only be generated from amplitudes with angles larger than 45°. Other properties of the heteronuclear NOE can be extracted from Equation 11b: In case the homonuclear interactions are neglected, it is obvious that the NOE depends neither on the number n of directly $^{13}C^{\beta}$ bound protons nor on a geometry factor like a bond length. Because of this characteristic feature, the heteronuclear NOE seems to be a suitable parameter describing the flexibility of side chains. The possible $^{1}H/^{13}C$ NOE values are supposed to range between 1.16 and 3. The largest value measured in RNase T1 amounts to 2.35 for $^{13}C^{\delta}$ of Lys[25]. Following the classification of homonuclear NOEs for structure calculations, we propose a distribution of heteronuclear NOEs in three classes (Table 1). While a lower limit for the amplitude of motion can be derived from a given NOE value, an upper limit cannot be determined. In particular, when the internal correlation time is very small or very large, small NOE values can also be generated from motions with large amplitudes. Thus, for a quantitative analysis T_1 relaxation times have to be included. Using the combination of these two experimental values, more realistic microdynamical parameters $\gamma_{\max}$ and τ_i may be obtained.

Cross-correlated cross-relaxation rate

While the cross correlation of the two CH vectors complicates more or less the determination of the T_1 relaxation time and the heteronuclear NOE, this contribution itself contains information about dynamical processes. A major problem of this quantity concerns its experimental determination. One possible method is connected with the different relaxation properties of the inner and outer lines of a CH_2 multiplet (Daragan et al., 1993; Daragan and Mayo, 1993b). Owing to signal overlap and line broadening because of the ^{13}C-^{13}C coupling in a uniformly ^{13}C-enriched protein, this technique is limited to small unlabelled molecules. For proteins the measurement of the heteronuclear cross-correlated cross-relaxation rate constant between the $S_x I_z^1 I_z^2$ and the S_x spin fragment introduced by Ernst and Ernst (1994) seems to be more practicable. This 'SIIS cross-relaxation' process is caused by a correlated modulation of the dipolar vectors SI^1 and SI^2 through a stochastical process. The corresponding relaxation rate depends exclusively on the cross correlation:

$$\Gamma^{\theta}_{4S_x I_{1z} I_{2z}, S_x} = \frac{3}{20} \left(\frac{\mu_0}{4\pi} \right) \frac{(\gamma_S \gamma_I \hbar)^2}{r_{SI_1}^3 r_{SI_2}^3} \left[\frac{4}{3} \sin^2\theta J_{HCH}(0) + (1 + \cos^2\theta) J_{HCH}(\omega_S) \right] \quad (17)$$

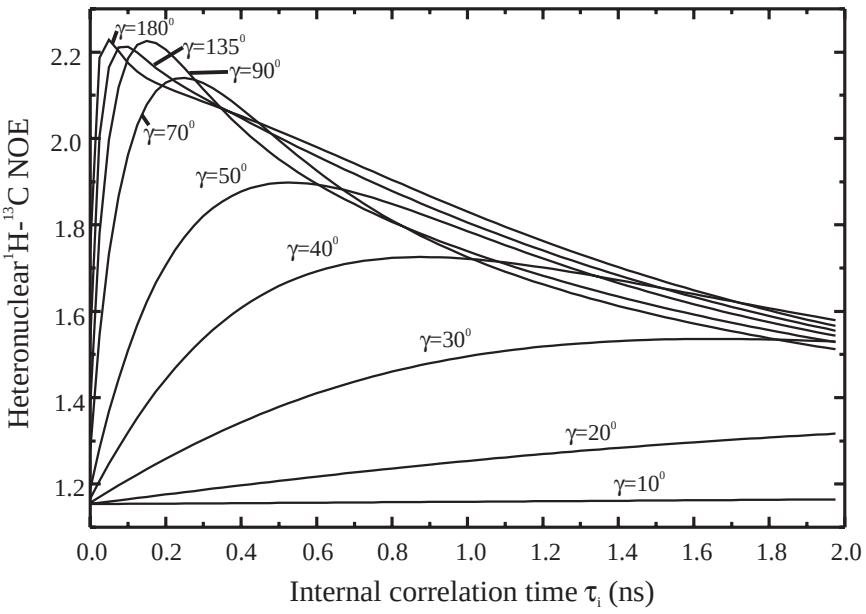

Figure 1. Theoretical steady-state $^{1}H/^{13}C$ NOE values for a β-CH_2 group as a function of the amplitude γ and the internal correlation time τ_i of the restricted rotational diffusion model. For the calculations, an overall correlation time τ_C of 5 ns and a ^{13}C resonance frequency of 125 MHz were assumed.

Table 1. Criteria for the classification of motions of CH and CH_2 groups using the heteronuclear ^{1}H-^{13}C NOE value; the lower limit for the angular amplitude γ_{max} stems from the restricted diffusion model

NOE	Classification	Lower limit for γ_{max} (°)
Lower than 1.4	Strongly restricted motion	0
1.4–1.8	Restricted but more flexible motion	23
Larger than 1.8	Highly flexible motion	42

where $J_{HCH}(\omega_S)$ is defined in Equations 7 and 14. The tilt angle θ of the rotating frame is given by $\tan\theta = \gamma_S B_1/\Delta\omega$, where $\gamma_S B_1$ is the amplitude of the ^{13}C spin-locking field and $\Delta\omega_S$ is the frequency offset. The transverse cross-relaxation rate constant for the restricted diffusion motion in dependence of the amplitude γ_{max} and the internal correlation time for an isotropic tumbling protein is shown in Figure 2. Since the tensor of inertia of RNase T1 has the principal components 1:1.14:1.27, it is reasonable to assume that it tumbles isotropically (Martinez-Oyanedel et al., 1991). Apparently for amplitudes smaller than 70 ° the sign of $\Gamma^{\pi/2}_{4S_xI_{1z}I_{2z},S_x}$ remains negative, independent of the internal correlation time. Only when the amplitude exceeds 70 ° the sign of $\Gamma^{\pi/2}_{4S_xI_{1z}I_{2z},S_x}$ depends on τ_i. For slow motions it will be negative and for fast motions it will be positive. Thus, the appearance of a negative cross peak in an SIIS cross-relaxation spectrum (due to a negative sign in the master equation, a negative cross-relaxation rate constant leads to a positive cross relaxation) indicates a high flexibility of the corresponding CH_2 group on a fast time scale. Hence, under certain conditions the SIIS cross-relaxation rate enables one to distinguish between a restricted motion and an unrestricted motion around the χ_1 dihedral angle already from the sign of the cross peak. Note that in proteins the experiment in the rotating frame is more favourable compared to the experiment in the laboratory frame, since the cross-relaxation constant is clearly larger and the zero point is shifted to smaller internal correlation times (Ernst and Ernst, 1994).

Besides the distinction of cross peaks between those with positive and negative amplitudes, a more detailed classification can be carried out using their

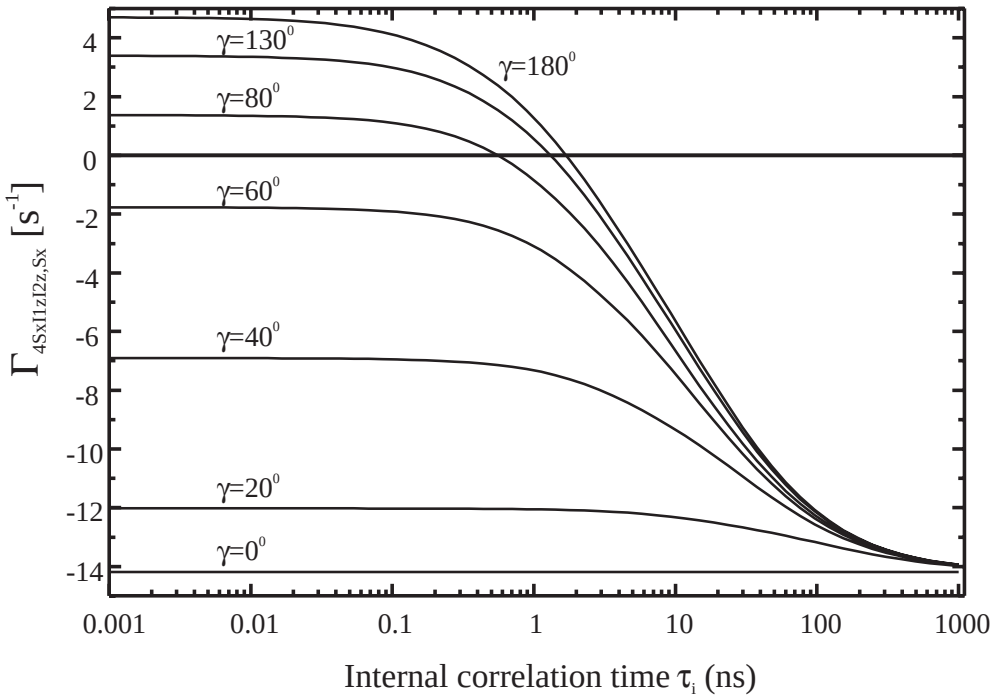

Figure 2. Theoretical SIIS cross-relaxation rate constant of a β-CH_2 group as a function of the amplitude γ and the internal correlation time τ_i of the restricted rotational diffusion model. For the calculations, an overall correlation time τ_C of 5 ns and a ^{13}C resonance frequency of 125 MHz were assumed.

intensities. Therefore, the pulse sequence specific influence of the magnetization transfer to the amplitude of the cross peak has to be considered. This problem may be overcome with recording a reference spectrum.

Experimental procedures

NMR spectroscopy

NMR experiments were performed on a Bruker DMX500 spectrometer, equipped with a triple-resonance $^{13}C/^{15}N/^{1}H$ probe head, operating at 313 K. Uniformly $^{15}N/^{13}C$-enriched RNase T1 was dissolved in H_2O to a final concentration of 2 mM, the pH being adjusted to 5.5.

Pulse sequences used to determine the relaxation rates

The pulse sequences developed for measuring the T_1 relaxation time and the heteronuclear $^{1}H/^{13}C$ NOE of the ^{13}C nuclei in the aliphatic side chains of proteins are depicted in Figure 3. They are based on the HCCONH experiment developed by Grzesiek et al. (1993) with modifications concerning the first part of the original pulse sequence. For measuring the longitudinal relaxation time, the magnetization was transferred from the aliphatic protons to the directly bound carbons using a refocused INEPT sequence. A period for the evolution of the carbon chemical shift followed. For determining T_1, the inversion recovery scheme was used. In order to minimize cross-correlation effects between the ^{1}H-^{13}C dipolar and CSA interaction, ^{1}H 180° pulses were applied every 5 ms (Boyd et al., 1990; Kay et al., 1992). Phase alternation of Φ5 leads to a magnetization decay of the form $\exp(-t/T_1)$. In this way, a less optimal delay between scans will only affect the sensitivity of the experiment, without introducing systematic errors (Sklenář et al., 1987). Subsequently, the magnetization was transferred by a coherent magnetization transfer from the $^{13}C^{\delta}$, $^{13}C^{\gamma}$, and $^{13}C^{\beta}$ nuclei to the $^{13}C^{\alpha}$ nucleus using the FLOPSY-8 pulse scheme (Mohebbi and Shaka, 1991). Finally, the magnetization was transferred to the $^{1}H^{N}$ proton of the following residue for detection using the carbonyl carbon and the ^{15}N nucleus as relay nuclei. In order to obtain T_1 relaxation rates, seven spectra were acquired with T delays of 10, 40, 80, 120, 180, 260 and 400 ms. For the evaluation of relaxation times, the intensities were fitted to a single exponential, depending on the relaxation delay. The

fit was performed using a least-squares minimization procedure based on a downhill-simplex algorithm and the margin of errors was determined by a Monte Carlo approach, using the method of simulated experimental data.

In order to determine ^{1}H-^{13}C NOEs, the first refocused INEPT sequence was dropped. Instead data sets with and without ^{1}H saturation were collected. Figure 3B indicates the sequence used for the data set with ^{1}H saturation. In this case a relaxation delay of 2.5 s was used, followed by proton presaturation during 3 s prior to the first 90 ° ^{13}C pulse. For spectra with missing NOEs, a delay of 5.5 s was employed between scans. NOE values were obtained from the ratio of two peak intensities recorded with and without presaturation. The margin of errors was determined according to Nicholson et al. (1992).

All data sets were recorded as 160×1024 real matrices with 64 scans per t_1 point and spectral widths of 8045 Hz in F1 and 6000 Hz in F2. Apodization, zero-filling and Fourier transformation resulted in a digital resolution of 8 Hz/point in the F1 and 2.9 Hz/point in the F2 dimension. The spectra were processed and analysed on a Silicon Graphics workstation using the XWINNMR and AURELIA programs (Bruker Analytische Messtechnik GmbH, Karlsruhe).

For the determination of the SIIS cross relaxation a density operator which is proportional to $S_xI_{z^1}I_{z^2}$ is generated and the time evolution of the S_x operator is observed. The original pulse sequence from Ernst and Ernst (1994) is shown in Figure 4A. Starting with longitudinal proton magnetization, the desired three-spin operator is generated prior to the mixing time with the depicted pulse scheme and is selected with a suitable phase cycle in combination with a triple quantum filter. The selection of the S_x term after the mixing time is obtained by detection of the S spin with simultaneous proton decoupling. As a consequence, all undesired terms of the density operator were suppressed. A sensitivity enhancement of this experiment was obtained when the S_x magnetization could be transferred back to the aliphatic protons for detection. However, for this reverse polarization transfer a complete suppression of all terms in the density matrix except the desired S_x is required. Such a selection of the undesired terms could not yet be realized experimentally.

The improved pulse sequence for measuring the SIIS cross relaxation is depicted in Figure 4B and represents a combination of the pulse scheme shown in Figure 4A and the CCONH type of magnetization transfer. After the mixing time, the direct evolution period for the ^{13}C nucleus is substituted by an indirect evolution period and subsequently the magnetization is transferred to the amide proton of the following residue in the same manner as in the T_1 and NOE experiments. In order to suppress all undesired terms of the density operator, in particular the $S_xI_{z^1}I_{z^2}$ term, the protons were decoupled as soon as the magnetization reaches the ^{15}N nucleus. This sequence is called SIIS-CCONH pulse sequence and has several advantages in comparison to the original experiment. The assignment of the resonance in the spectrum is quite simple, since the positions of the cross peaks are the same as in the frequently used spectra for side chain assignments (Grzesiek et al., 1993). Furthermore, the sensitivity of the experiment is higher due to the ^{1}H detection.

In both SIIS experiments, a spin-lock field with an amplitude of 5000 Hz and a duration of 25 ms was used. In order to obtain an optimal transfer for $^{13}CH_2$ groups, the delay τ was adjusted to 1.666 ms. In experiment (A) 88 t_1 increments with 5632 scans and 2048 real data points each were acquired using about 144 h of instrument time. The spectral width in the indirect proton dimension amounts to 1900 Hz. In experiment (B) a 160×2048 real matrix with 1920 scans was recorded, giving rise to a total acquisition time of approximately 72 h. Spectral width was set to 8000 Hz in the indirect ^{13}C dimension, yielding a digital resolution of 50 Hz/point in the F1 dimension.

Results and discussion

SIIS cross relaxation

Most of the $^{13}CH_2$ cross peaks in the SIIS cross-relaxation spectra have a positive sign. Using the original SIIS pulse sequence, resonances with negative amplitudes are only obtained for the $^{13}CH_2$ groups of β-Ser^{13}, β-Ser^{14}, β-Ser^{96}, β- and γ-Pro^{55} and the γ-, δ- and ϵ-CH_2 groups of Lys^{25} and Lys^{41} (Figure 5). The negative cross peaks for Pro^{55} can be explained with a rapid ring-puckering process with approximate correlation times of $\sim$30 ps. The three other proline residues (Pro^{39}, Pro^{60} and Pro^{73}) in RNase T1 do not appear in the spectrum. The negative cross peaks of the β-$^{13}CH_2$ groups of Ser^{13}, Ser^{14} and Ser^{96} suggest that the rotation around χ_1 is less restricted in its angular range ($\geq$70 °) and is rapid with a correlation time $\tau_i < 0.335\tau_C \approx 1.8$ ns. The negative cross peaks of the lysine side chain carbons indicate a rapid and virtually unrestricted motion of these side chains, implying

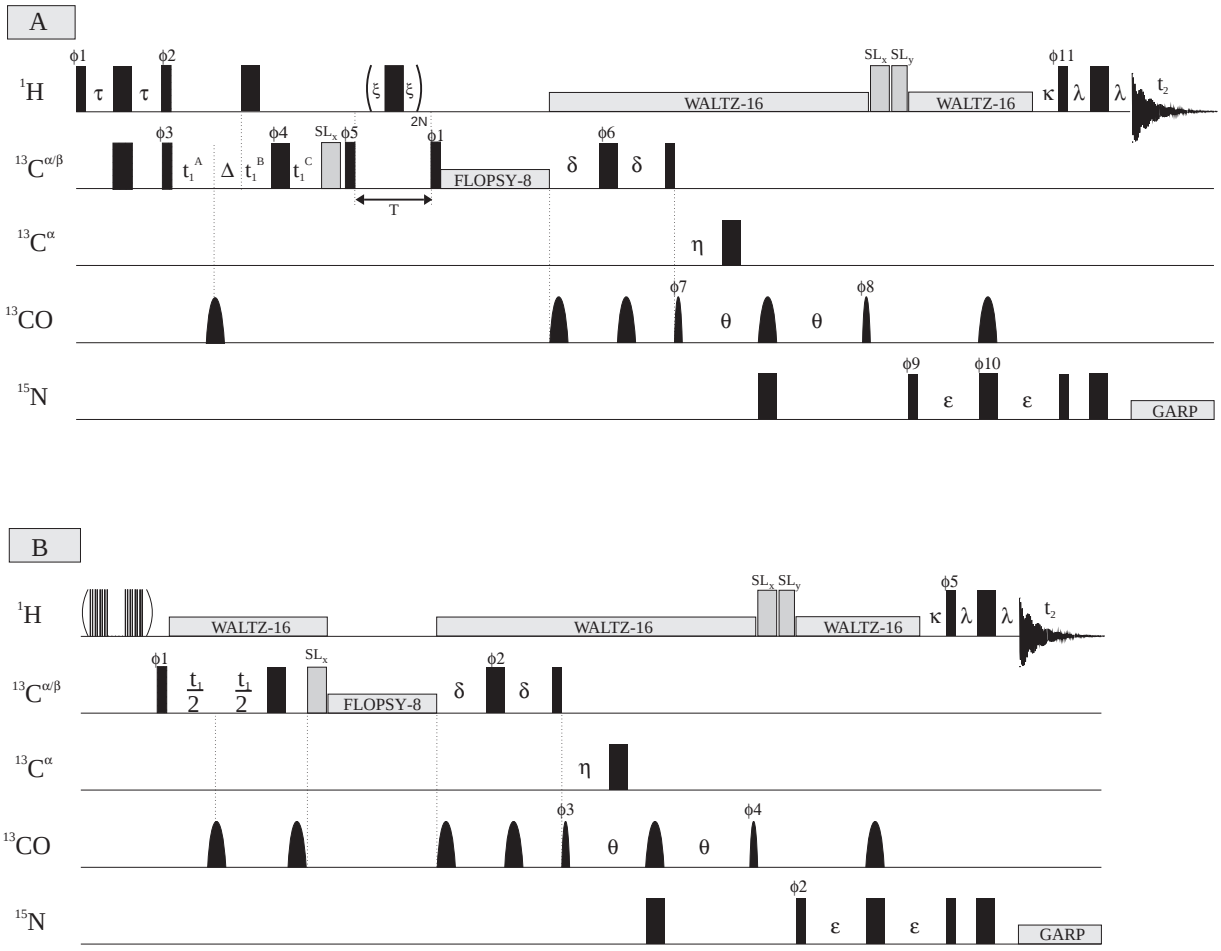

Figure 3. Pulse sequences used for the measurement of ^{13}C T_1 (A) and NOE values (B) with ^{1}H detection. All narrow pulses had a flip angle of 90°; the larger pulses had a 180° flip angle. Pulses for which the phase is not indicated were applied along the x-axis. Spin-lock ^{1}H pulses (SL) of a duration of 3 ms and 1.2 ms were applied along the x-axis and y-axis, respectively, to suppress the residual water signal and magnetization originating from protons not directly coupled to ^{13}C. At the beginning of the experiment, the carrier frequency in the ^{13}C channel was adjusted to 43 ppm and was switched after the last ^{13}C 90° pulse to the $^{13}C^{\alpha}$ region (56 ppm). The power of the 90° and 180° $^{13}C^{\alpha}$ pulses was adjusted such that they did not excite the $^{13}C'$ nuclei ($\tau^{90} = \sqrt{15}/(4\,\Delta\nu)$ and $\tau^{180} = \sqrt{3}/(2\,\Delta\nu)$ with $\Delta\nu$ =15.2 kHz). The strength of the ^{13}C spin-lock pulse was 9450 Hz and its duration was set to 1 ms. For the coherent ^{13}C magnetization transfer, a FLOPSY-8 sequence with an rf field strength of 7 kHz and a duration of 12 ms was applied. In order to start and end the mixing sequence with z-magnetization, two 90° ^{13}C pulses have to be applied at the beginning and end of the mixing sequence. Sinc-shaped phase-modulated off-resonance DANTE pulses with an rf field strength of 2500 Hz for the 180° pulses and 1250 Hz for the 90° pulses were used to excite the carbonyl carbons 120 ppm downfield from the ^{13}C carrier. ^{1}H and ^{15}N decoupling was accomplished using the WALTZ-16 and GARP sequences, with a field of 1800 Hz and a 900 Hz rf field, respectively. Delay durations were: $\tau = 1.5$ ms, $\Delta = 1.05$ ms, $t_1^A = t_1^B = 0$, $t_1^C = 1.05$ ms, $\xi = 5$ ms, $\delta = 3.2$ ms, $\eta = 4.5$ ms, $\theta = 11.4$ ms, $\epsilon = 12$ ms, $\kappa = 5.4$ ms, $\lambda = 2.25$ ms. For the ^{13}C evolution period, the delays t_1^A, t_1^B and t_1^C were incremented in a semi-constant time manner (Farrow et al., 1994). Phase cycling used was as follows: (A) $\Phi1$ = y; $\Phi2$ = x, –x; $\Phi3$ = x; $\Phi4$ = 8(x),8(y),8(–x),8(–y); $\Phi5$ = 32(y),32(–y); $\Phi6$ = 4(x),4(–x); $\Phi7$ = 2(x),2(–x); $\Phi8$ = 25° (Bloch–Siegert phase error compensation); $\Phi9$ = 4(x),4(–x); $\Phi10$ = 8(x),8(–x); $\Phi11$ = 16(x),16(–x); rec. = P,–P,–P,P,–P,P,P,–P with P = x,–x,–x,x. The receiver phase is inverted after 32 scans. (B) $\Phi1$ = 8(y),8(–y); $\Phi2$ = 4(x),4(–x); $\Phi3$ = 2(x),2(–x); $\Phi4$ = 25°; $\Phi5$ = x,–x; rec. = (x,–x,–x,x),2(–x,x,x,–x),(x,–x,–x,x), Quadrature detection is achieved by a TPPI of $\Phi3$ for scheme (A) and $\Phi1$ for scheme (B).

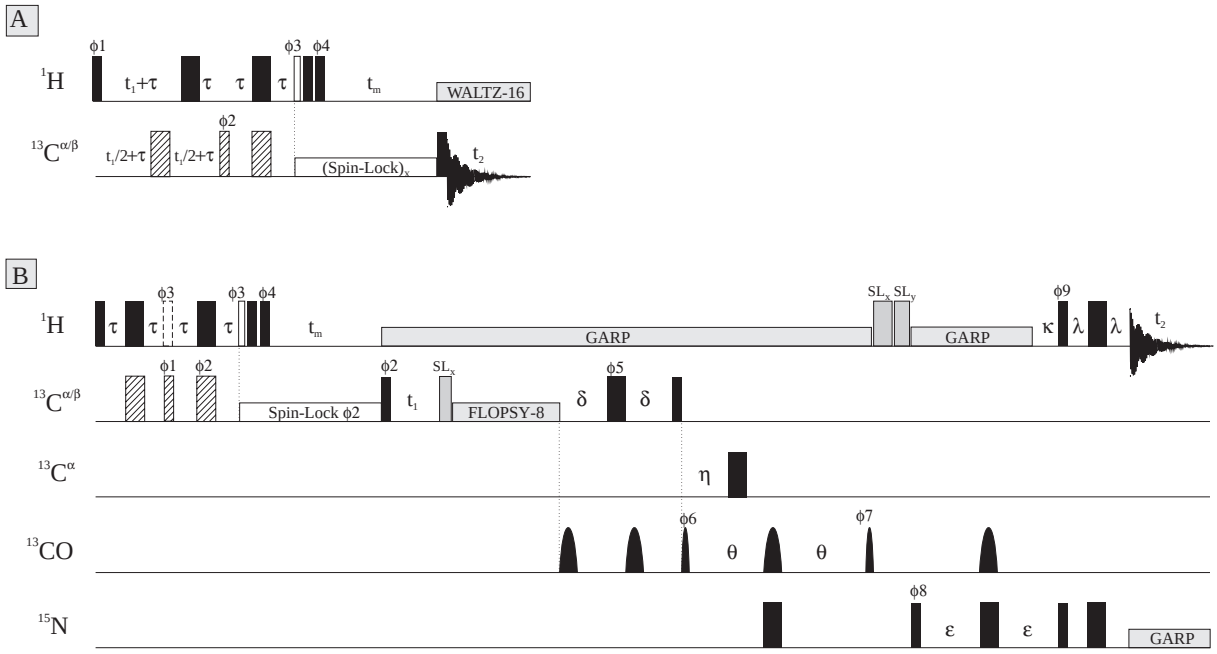

Figure 4. Pulse sequences used for the measurement of transverse SIIS cross relaxation. The original pulse sequence of Ernst and Ernst with detection of the carbon magnetization is shown in (A). The ^{13}C carrier frequency in this experiment is adjusted to 43 ppm and the rf field strength of the ^{13}C pulses was set to 25 kHz (indicated by hatched pulses). For ^{1}H decoupling during acquisition, a WALTZ-16 sequence with a field strength of 3125 Hz was used. The ^{1}H pulse with the phase Φ3 rotates the magnetization by 45 °. In (B) the SIIS-CCONH pulse sequence is shown, whereby the first part up to the ^{13}C pulse with the phase Φ2 is identical to the pulse scheme in (A). The frequency, pulse and decoupling conditions are identical to the T_1 and NOE experiment shown in Figure 3. Delay durations were: τ = 1.666 ms, t_m = 25 ms. Phase cycling used was as follows: (A) Φ1 = x,–x; Φ2 = 4(x),4(–x); Φ3 = 2(y),2(–y); Φ4 = 8(x),8(y),8(–x),8(–y); rec. = (x,–x,–x,x),2(–x,x,x,–x),(x,–x,–x,x). (B) Φ1 = 8(x),8(–x); Φ2 =x; Φ3 = 16(y),16(–y); Φ4 = 32(x),32(y); Φ5 = 4(x),4(–x); Φ6 = 2(x),2(–x); Φ7 = 25 ° (Bloch–Siegert phase error compensation); Φ8 =x,–x; rec. = P,–P,–P,P,–P,P,P,–P with P = x,–x,–x,x. The receiver phase is inverted after 32 scans. Quadrature detection is achieved by a TPPI of Φ1 for scheme (A) and Φ1 and Φ2 for scheme (B). In order to record the reference INEPT-CCONH spectrum, the dashed 90 ° ^{1}H pulse with phase Φ3 is inserted in the pulse sequence while the triple quantum filter is removed. In addition, the receiver phase is not inverted after 32 scans.

that the NH_3 group sticks out into solution and does not undergo intramolecular hydrogen bonding.

The SIIS spectrum recorded with the SIIS-CCONH pulse scheme is shown in Figure 6. Although the spectrum is acquired in half of the spectrometer time necessary for the spectrum in Figure 5, the dispersion of the signals is much better, more resonances are visible and the signal intensities are generally higher. The signs of the resonances observed in both spectra agree without exception, which seems to be a confirmation for the validity of the new pulse sequence. Additional cross peaks with a negative amplitude are obtained from this spectrum for the β-CH_2 groups of Ser^{17}, Ser^{53}, Asp^{49} and Asn^{98}. As mentioned before, the measurement of transverse ^{13}C relaxation times in a uniformly ^{13}C-enriched protein is difficult due to the Hartmann–Hahn magnetization transfer during the spin-lock pulse (Hartmann and Hahn, 1962). The same effect will be present in the SIIS experiment, leading to the following dependence of the cross-peak intensity:

$$I \sim \sinh(\Gamma^{\theta}_{4S_x I_{1z} I_{2z}, S_x}\, t_m)\; e^{-t_m/T_2}\, \lambda(\Omega_1, \Omega_2, \gamma B_1, t_m) \qquad (18)$$

where T_2 is the transverse relaxation time, t_m is the length of the spin-lock pulse and γB_1 the spin-lock field strength. λ characterizes the decrease of magnetization due to the Hartmann–Hahn transfer which depends on the chemical shift of the two adjacent nuclei and the length and strength of the spin-lock pulse. This contribution may lead to serious problems for a quantitative analysis of the cross-peak intensity so that only a distinction in cross peaks of positive and negative signs is reasonable.

For a further quantitative interpretation the specific influence of the pulse sequence and the Hartmann–Hahn transfer to the absolute cross-peak intensity has

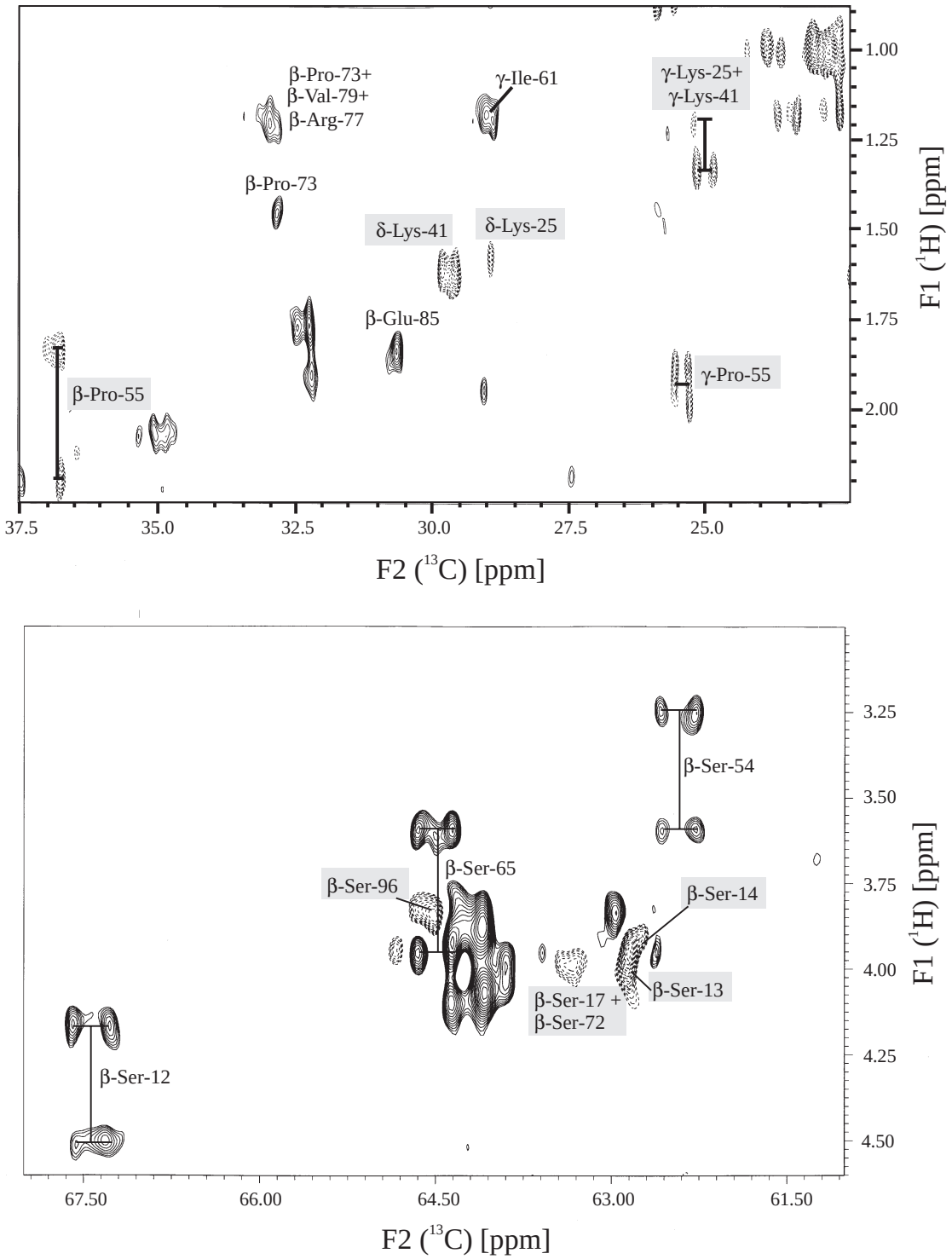

Figure 5. Two different parts of the 2D-SIIS spectrum of RNase T1, recorded with the pulse sequence of Figure 4A. Negative intensities are indicated by broken contour lines. Experiment time: 6 days.

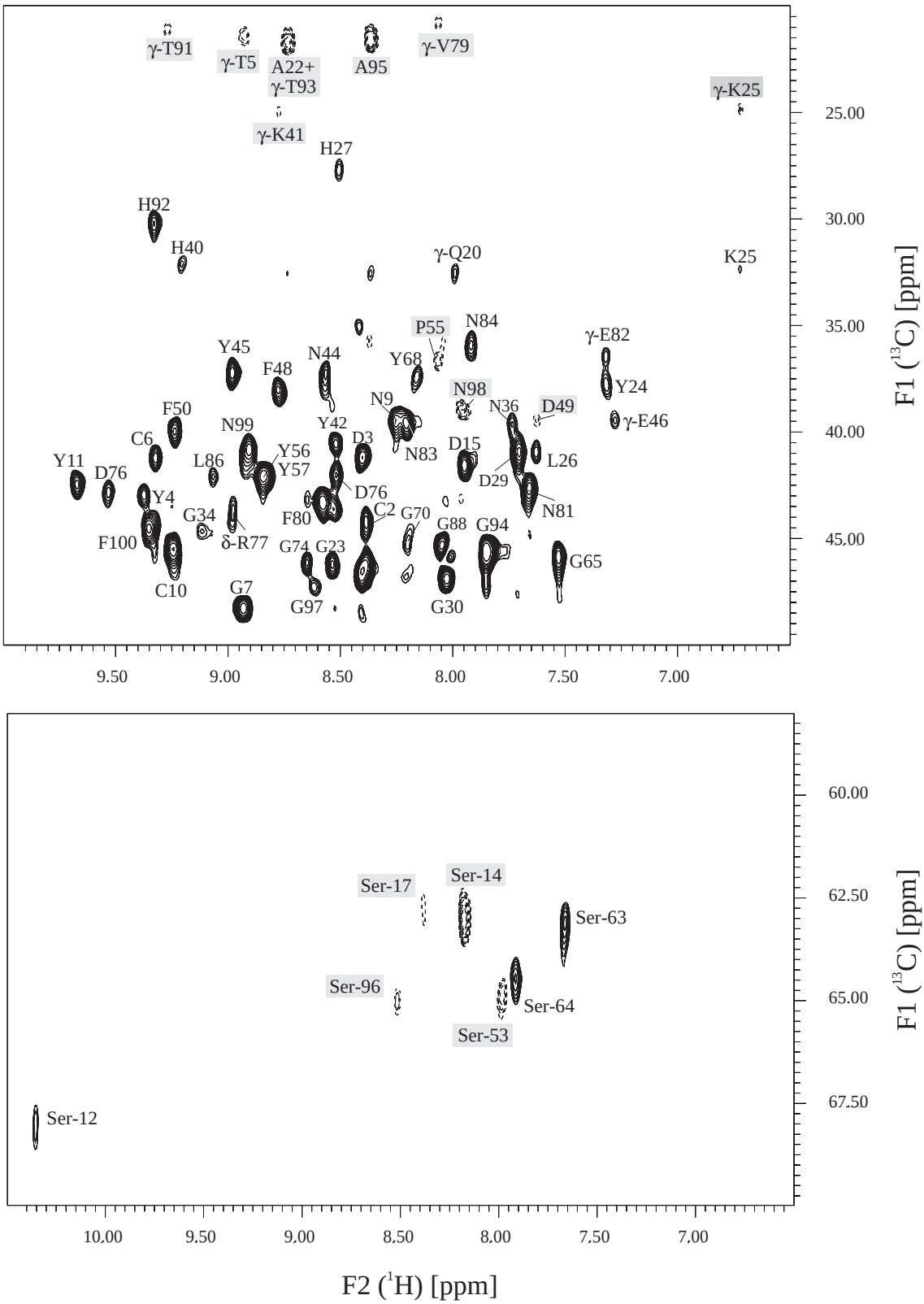

Figure 6. Two different parts of the 2D-SIIS spectrum of RNase T1, recorded with the pulse sequence of Figure 4B. Negative intensities are indicated by broken contour lines. Experiment time: 3 days.

Table 2. Criteria for the classification of motions of β-CH_2 groups using the cross-peak intensities in the SIIS-CCONH and INEPT-CCONH spectra

Intensity in the INEPT-CCONH spectrum I_I	Intensity in the SIIS-CCONH spectrum I_S	Ratio I_S/I_I	Classification of the motion
High	High	0.4 to 1	Strongly restricted motion
Low	Low	0.4 to 1	Strongly restricted motion
High	Low or Cannot be determined	0 to 0.4	Restricted but more flexible motion
Low	Not measurable	–	Not determined
Positive	Negative	–1 to 0	Highly flexible motion

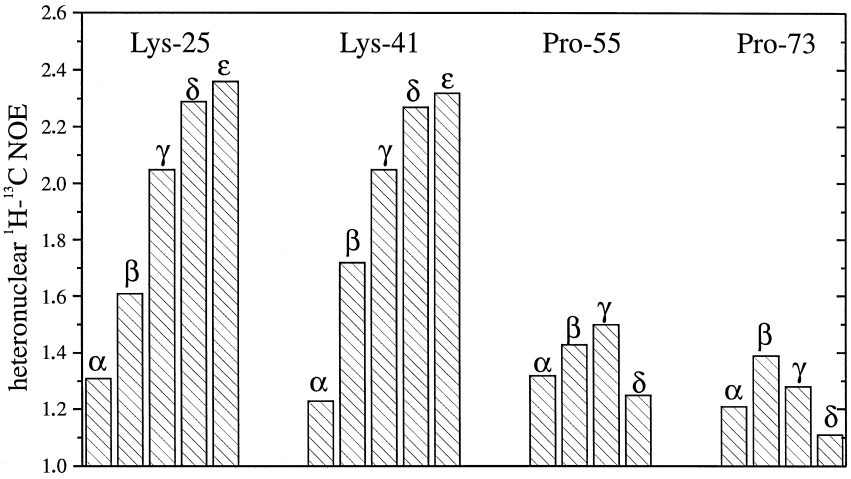

Figure 7. Heteronuclear ^{1}H-^{13}C NOE values for Lys^{25}, Lys^{41}, Pro^{55} and Pro^{73}.

to be considered. This normalization is obtained by recording a reference spectrum in which the SIIS part of the SIIS-CCONH pulse sequence is substituted by a refocused INEPT scheme. The intensity of the cross peaks in the reference spectrum is given by

$$I \sim e^{-t_m/T_2}\,\lambda(\Omega_1, \Omega_2, \gamma B_1, t_m) \qquad (19)$$

The ratio of both cross-peak intensities allows an estimate of the relative size of the cross-relaxation rate constant, since the influence of the magnetization loss due to the Hartmann–Hahn effect and the transverse relaxation is the same in both cases. In case the amplitude is positive and large in both spectra, the motion of the $^{13}CH_2$ group is either rapid and strongly restricted in the amplitude or slow with an internal correlation time longer than ≈1.8 ns. Cross peaks with a large amplitude in the INEPT-CCONH spectrum and a small amplitude in the SIIS-CCONH spectrum indicate an increased mobility. Note that the ratio of intensities is independent of the value of the transverse relaxation time, since it affects the cross peaks in both spectra in the same manner and thus is cancelled out. Possible combinations as well as the implications of the data with respect to the flexibility are summarized in Table 2. Using these criteria, the dynamics of 53 out of 68 β-$^{13}CH_2$ groups in RNase T1 have been divided into three classes with corresponding amplitudes of motions:

(1) *Strongly restricted motion:* Asp^3, Tyr^4, Cys^6, Cys^{10}, Tyr^{11}, Ser^{12}, Asp^{15}, Tyr^{24}, Leu^{26}, His^{27}, Asp^{29}, His^{40}, Tyr^{42}, Asn^{43}, Asn^{44}, Tyr^{45}, Phe^{48}, Phe^{50}, Ser^{63}, Ser^{64}, Tyr^{68}, Asp^{76}, Phe^{80}, Asn^{81}, Asn^{84}, Leu^{86}, His^{92}, Asn^{99}, Phe^{100}.

(2) *Restricted (medium-sized) motion:* Cys^2, Ser^8, Asn^9, Lys^{25}, Glu^{28}, Glu^{31}, Asn^{36}, Ser^{37}, Lys^{41}, Ser^{51}, Glu^{58}, Asp^{66}, Glu^{82}, Asn^{83}, Gln^{85}, Glu^{102}.

Table 3. Summary of the longitudinal relaxation times and the heteronuclear NOE values of the ^{13}C aliphatic side chain nuclei of RNase T1. In addition, the microdynamical parameters γ_{max} and τ_i as well as the normalized SIIS cross-relaxation rate for the $^{13}C^{\beta}$ nucleus are shown

Residue	C^{β}, C^{δ}		C^{γ}, C^{ϵ}		Normalized	Parameters of motion	
	T_1 (ms)	NOE	T_1 (ms)	NOE	SIIS rate	γ_{max}	τ_i (ns)
Cys^{2}	232 ± 8	1.56 ± 0.08	–	–	0.36	35 ± 6	0.751 ± 0.385
Asp^{3}	216 ± 14	1.22 ± 0.06	–	–	0.74	5 ± 4	0.275 ± 0.048
Tyr^{4}	244 ± 4	1.27 ± 0.06	–	–	0.61	27 ± 4	0.457 ± 0.254
Thr^{5}	521 ± 37	1.27 ± 0.06	SI_3	SI_3	SI	37 ± 4	0.150 ± 0.045
Cys^{6}	225 ± 9	1.27 ± 0.06	–	–	0.58	17 ± 4	3.475 ± 3.416
Ser^{8}	190 ± 8	1.77 ± 0.09	–	–	<0.3	46 ± 6	1.026 ± 0.362
Asn^{9}	233 ± 6	1.38 ± 0.07	–	–	0.32	28 ± 9	0.802 ± 0.210
Cys^{10}	307 ± 20	1.24 ± 0.06	–	–	0.79	38 ± 5	0.073 ± 0.117
Tyr^{11}	276 ± 7	1.20 ± 0.06	–	–	0.67	32 ± 4	0.082 ± 0.056
Ser^{12}	290 ± 8	1.46 ± 0.07	–	–	0.5	42 ± 4	0.201 ± 0.037
Ser^{13}	OV	OV	–	–	neg	–	–
Ser^{14}	OV	OV	–	–	neg	–	–
Asp^{15}	311 ± 30	1.31 ± 0.07	–	–	0.65	43 ± 7	0.090±0.024
Val^{16}	578 ± 22	1.20 ± 0.06	SI_3	SI_3	SI	45 ± 3	0.038 ± 0.022
Ser^{17}	OV	OV	–	–	neg.	–	–
Thr^{18}	541 ± 57	1.25 ± 0.06	SI_3	SI_3	SI	38 ± 10	0.105 ± 0.038
Gln^{20}	367 ± 60	1.21 ± 0.06	334±31	1.24 ±0.06	LI	48 ± 11	0.020 ± 0.012
Tyr^{24}	247 ± 25	1.20 ± 0.06	–	–	0.92	25 ± 3	1.231 ± 0.287
Lys^{25}	280 ± 9	1.61 ± 0.08	309 ± 9	2.05 ± 0.10	0.36	48 ± 4	0.213 ± 0.042
	384 ± 7	2.29 ± 0.11	497 ± 8	2.36 ± 0.12			
Leu^{26}	371 ± 54	1.20 ± 0.06	LI	LI	1	49 ±4	0.017± 0.014
His^{27}	297 ± 23	1.30 ± 0.07	–	–	0.5	40 ± 5	0.111 ± 0.037
Glu^{28}	294 ± 15	1.66 ± 0.08	314 ± 8	1.71 ±0.1	<0.3	49 ± 4	0.192 ± 0.060
Asp^{29}	329 ± 22	1.34 ± 0.07	–	–	0.68	47 ± 4	0.078± 0.053
Glu^{31}	265 ± 17	1.82 ± 0.09	285 ± 5	1.88 ± 0.09	<0.3	55 ± 5	0.240 ± 0.102
Thr^{32}	486 ± 34	1.22 ± 0.06	SI_3	SI_3	SI	30 ± 4	0.201 ± 0.103
Val^{33}	365 ± 12	1.59 ± 0.08	SI_3	SI_3	SI	38 ± 5	1.163 ± 0.257
Asn^{36}	287 ± 26	1.90 ± 0.10	–	–	<0.3	62 ± 5	0.175 ± 0.076
Ser^{37}	348 ± 20	1.59 ± 0.08	–	–	<0.3	55 ± 4	0.105 ± 0.024
Pro^{39}	OV	OV	OV	1.18 ± 0.06	–	–	–
	305 ± 19	1.23 ± 0.07					
His^{40}	287 ± 11	1.25 ± 0.06	–	–	0.51	37 ± 4	0.105 ± 0.057
Lys^{41}	210 ± 18	1.74 ± 0.09	281 ± 14	2.06 ± 0.10	0.32	43 ± 5	0.727 ± 0.454
	408 ± 15	2.27 ± 0.11	428 ± 30	2.32 ± 0.12			
Tyr^{42}	242 ± 14	1.27 ± 0.06	–	–	0.78	26 ± 4	0.526 ± 0.265
Asn^{43}	304 ± 19	1.33 ± 0.07	–	–	0.59	42 ± 5	0.109 ± 0.086
Asn^{44}	295 ± 24	1.12 ± 0.06	–	–	0.45	ND	ND
Tyr^{45}	289 ± 25	1.28 ± 0.06	–	–	0.76	38 ± 5	0.119 ± 0.043
Glu^{46}	317 ± 25	1.40 ± 0.07	329 ± 19	1.42 ± 0.07	0.75	47 ± 5	0.106 ± 0.066
Phe^{48}	232 ± 28	1.33 ± 0.07	–	–	0.75	26 ± 3	0.914 ± 0.611
Asp^{49}	246 ± 10	1.97 ± 0.10	–	–	–0.08	60 ± 5	0.268 ± 0.064
Phe^{50}	306 ± 13	1.26 ± 0.06	–	–	0.67	40 ± 4	0.077 ± 0.019
Ser^{51}	249 ± 11	1.67 ± 0.08	–	–	0.05	43 ± 8	0.414 ± 0.153
Val^{52}	510 ± 12	1.24 ± 0.06	SI_3	SI_3	SI	38 ± 4	0.108 ± 0.032
Ser^{53}	189 ± 9	1.78 ± 0.09	–	–	–0.19	47 ± 8	1.002 ± 0.363
Ser^{54}	414 ± 32	1.34 ± 0.07	–	–	pos.	55 ± 5	0.037 ± 0.022
Pro^{55}	444 ± 21	1.43 ± 0.07	452 ± 30	1.50 ± 0.08	neg.	64 ± 3	0.036 ± 0.012
	342 ± 9	1.25 ± 0.06					

Table 3. Continued

Residue	C^{β}, C^{δ}		C^{γ}, C^{ϵ}		Normalized	Parameters of motion	
	T_1 (ms)	NOE	T_1 (ms)	NOE	SIIS rate	γ_{max}	τ_i (ns)
Glu^{58}	270 ± 32	1.39 ± 0.07	310 ± 8	1.82 ± 0.09	<0.3	38 ± 3	0.240 ± 0.050
Ile^{61}	463 ± 11	1.20 ± 0.06	348 ± 16	1.50 ± 0.08	SI	30 ± 5	0.178 ± 0.093
Leu^{62}	379 ± 43	1.36 ± 0.07	689 ± 6	1.67 ± 0.09	LI	54 ± 6	0.048 ± 0.010
Ser^{63}	277 ± 13	1.35 ± 0.07	–	–	0.63	36 ± 4	0.231 ± 0.117
Ser^{64}	310 ± 8	1.19 ± 0.06	–	–	0.52	39 ± 3	0.038 ± 0.022
Asp^{66}	249 ± 17	1.82 ± 0.09	–	–	0.29	52 ± 5	0.303 ± 0.043
Val^{67}	411 ± 14	1.44 ± 0.07	SI_3	SI_3	SI	33 ± 4	0.761 ± 0.211
Tyr^{68}	228 ± 32	1.24 ± 0.06	–	–	0.91	19 ± 3	1.401 ± 1.090
Ser^{69}	LI	1.39 ± 0.07	–	–	pos.	–	–
Pro^{73}	304 ± 35	1.39 ± 0.07	373 ± 8	1.28 ± 0.06	LI	44 ± 4	0.126 ± 0.016
	294 ± 23	1.10 ± 0.06					
Asp^{76}	338 ± 28	1.41 ± 0.07	–	–	0.57	50 ± 5	0.083 ± 0.054
Val^{78}	304 ± 6	1.47 ± 0.07	SI_3	SI_3	SI	48 ± 4	2.348 ± 0.425
Val^{79}	619 ± 25	1.26 ± 0.06	SI_3	SI_3	SI	51 ± 4	0.044 ± 0.039
Phe^{80}	297 ± 44	1.36 ± 0.07	–	–	0.95	42 ± 3	0.133 ± 0.024
Asn^{81}	303 ± 12	1.23 ± 0.06	–	–	0.64	39 ± 4	0.064 ± 0.040
Glu^{82}	182 ± 14	1.44 ± 0.07	200 ± 9	1.55 ± 0.08	<0.3	33 ± 3	3.387 ± 0.829
Asn^{83}	301 ± 25	1.72 ± 0.09	–	–	0.38	56 ± 6	0.159 ± 0.114
Asn^{84}	322 ± 47	1.14 ± 0.06	–	–	0.48	ND	ND
Gln^{85}	299 ± 9	1.45 ± 0.07	267 ± 10	1.43 ± 0.08	<0.3	45 ± 4	0.149 ± 0.037
Leu^{86}	296 ± 38	1.10 ± 0.06	429 ± 25	2.15 ± 0.11	0.5	ND	ND
Val^{89}	586 ± 41	1.37 ± 0.07	SI_3	SI_3	SI	52 ± 5	0.082 ± 0.052
Ile^{90}	478 ± 34	1.17 ± 0.06	LI	1.27 ± 0.06	SI	31 ± 48	0.083 ± 0.082
His^{92}	382 ± 48	1.23 ± 0.06	–	–	0.61	51 ± 5	0.022 ± 0.013
Thr^{93}	607 ± 67	1.27 ± 0.06	SI_3	SI_3	SI	46 ± 2	0.063 ± 0.020
Ser^{96}	236 ± 11	1.96 ± 0.10	–	–	neg.	56 ± 6	0.350 ± 0.085
Asn^{98}	274 ± 14	1.92 ± 0.10	–	–	–0.11	61 ± 5	0.200 ± 0.052
Asn^{99}	273 ± 10	1.42 ± 0.07	–	–	0.48	40 ± 4	0.231 ± 0.077
Phe^{100}	254 ± 33	1.38 ± 0.07	–	–	0.71	34 ± 6	0.365 ± 0.076
Val^{101}	428 ± 10	1.35 ± 0.07	SI_3	SI_3	SI	31 ± 6	0.592 ± 0.225
Glu^{102}	305 ± 20	1.71 ± 0.09	372 ± 15	1.96 ± 0.09	<0.3	56 ± 4	0.151 ± 0.046
Cys^{103}	291 ± 30	1.20 ± 0.06	–	–	OV	34 ± 3	0.085 ± 0.060

In order to calculate the confidence interval of the dynamical parameters, 200 'artificial experimental data sets' were generated using a Monte Carlo simulation.
ND: a value could not be determined; OV: cross peak is overlapped; LI: cross peak has low intensity; SI: SI spin system; SI_3: methyl group.

(3) *Unrestricted motion:* Ser^{13}, Ser^{14}, Ser^{17}, Asp^{49}, Ser^{53}, Pro^{55}, Ser^{96}, Asn^{98}.

The major advantage of the data is connected with its unambiguous character. By means of the sign of the cross peaks in the spectrum, a distinction between rigid and flexible side chains can easily be made. Such a clear-cut evidence is known for only very few methods used for investigating dynamical features of biological macromolecules.

T_1 and heteronuclear NOE

For a qualitative analysis of the motion of side chains, the heteronuclear $^1H/^{13}C$ NOE can be used. NOE values were obtained for 95 CH and CH_2 nuclei of the side chains of RNase T1. The range of NOE values varies between 1.10 for the $^{13}C^{\beta}$ nucleus of Leu^{86} and 2.36 for the $^{13}C^{\epsilon}$ nucleus of Lys^{25}. The values for the heteronuclear NOE of Lys^{25}, Lys^{41}, Pro^{55} and Pro^{73} are depicted in Figure 7. For the two lysine residues a continuing increase of the NOEs along the side chain was observed, indicating an increasing flexibility to

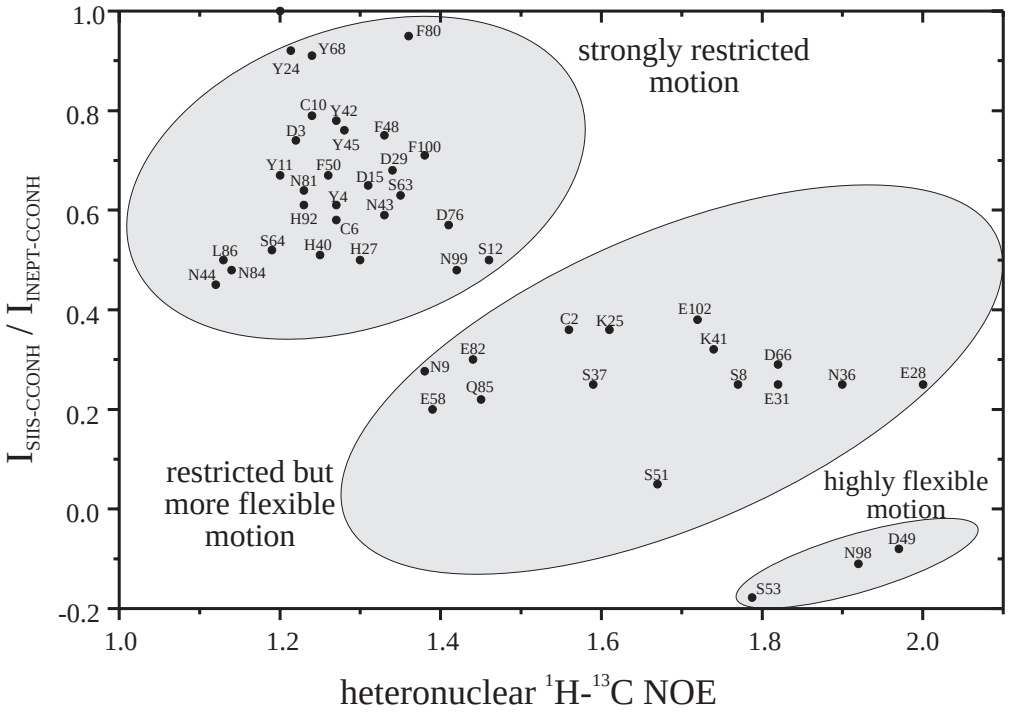

Figure 8. Correlation between the heteronuclear NOE and the normalized SIIS cross-peak intensity for the β-CH_2 groups of RNase T1. The three possible areas of motion are indicated.

the end of the side chain. The corresponding $^{13}C^{\epsilon}$ nuclei reveal the largest NOE value of all CH and CH_2 groups. This result agrees well with the SIIS cross-relaxation rates. In fact, negative cross peaks were observed for these side chain nuclei. For the two proline residues smaller NOE values compared with the lysine residues were observed. Clearly different values were determined for their $^{13}C^{\gamma}$ nuclei, whereby the NOE value for Pro^{55} is significantly larger than that of Pro^{73}. This result is a further indication for the puckering motion of the prolyl ring of Pro^{55}.

A comparison between the NOE values and the normalized SIIS cross-relaxation rate for $^{13}CH_2$ groups is shown in Figure 8. It is obvious that a clear correlation between these two values exists: the larger the NOE values, the smaller the amplitude in the SIIS cross-relaxation spectrum. In Figure 8 three different classes of side chain mobility could be identified. All $^{13}C^{\beta}$ nuclei with a normalized SIIS resonance amplitude larger than 0.4 have a NOE value between 1.12 and 1.5. Hence, their flexibility is assumed to be strongly restricted. Side chains of which the $^{13}C^{\beta}$ nucleus has a positive but smaller SIIS resonance amplitude are obviously more flexible. A nearly isotropic motion is expected for $^{13}CH_2$ side chain groups with a NOE value larger than 1.8 and a negative cross peak in the SIIS spectrum.

In the quantitative analysis of the motion of the $^{13}C^{\beta}$ nucleus, the T_1 relaxation time and the heteronuclear NOE were included. Both relaxation rates were determined for 70 out of 85 $^{13}C^{\beta}$ nuclei of RNase T1 (glycine and alanine residues excepted). However, in the analysis only those relaxation rates were considered whose margins of error were smaller than 10%. In total, microdynamical parameters could be calculated for 67 β-CH and β-CH_2 groups, assuming an overall correlation time of 4.8 ns determined by ^{15}N relaxation time measurements of the same sample. For the calculation, the specific type of the side chain was considered, i.e. the contributions of all directly $^{13}C^{\beta}$ bound protons and carbons were taken into account. In addition, the influence of the $^{1}H^{\alpha}$ nucleus was considered by using the model-free approach of Lipari and Szabo (1982a) with an order parameter of 0.8. The results of these investigations are summarized in Table 3.

For a β-CH_2 group which is bound to two adjacent ^{13}C nuclei the angular amplitude and the internal correlation time in dependence of the T_1 relaxation time and the heteronuclear NOE are shown in the contour

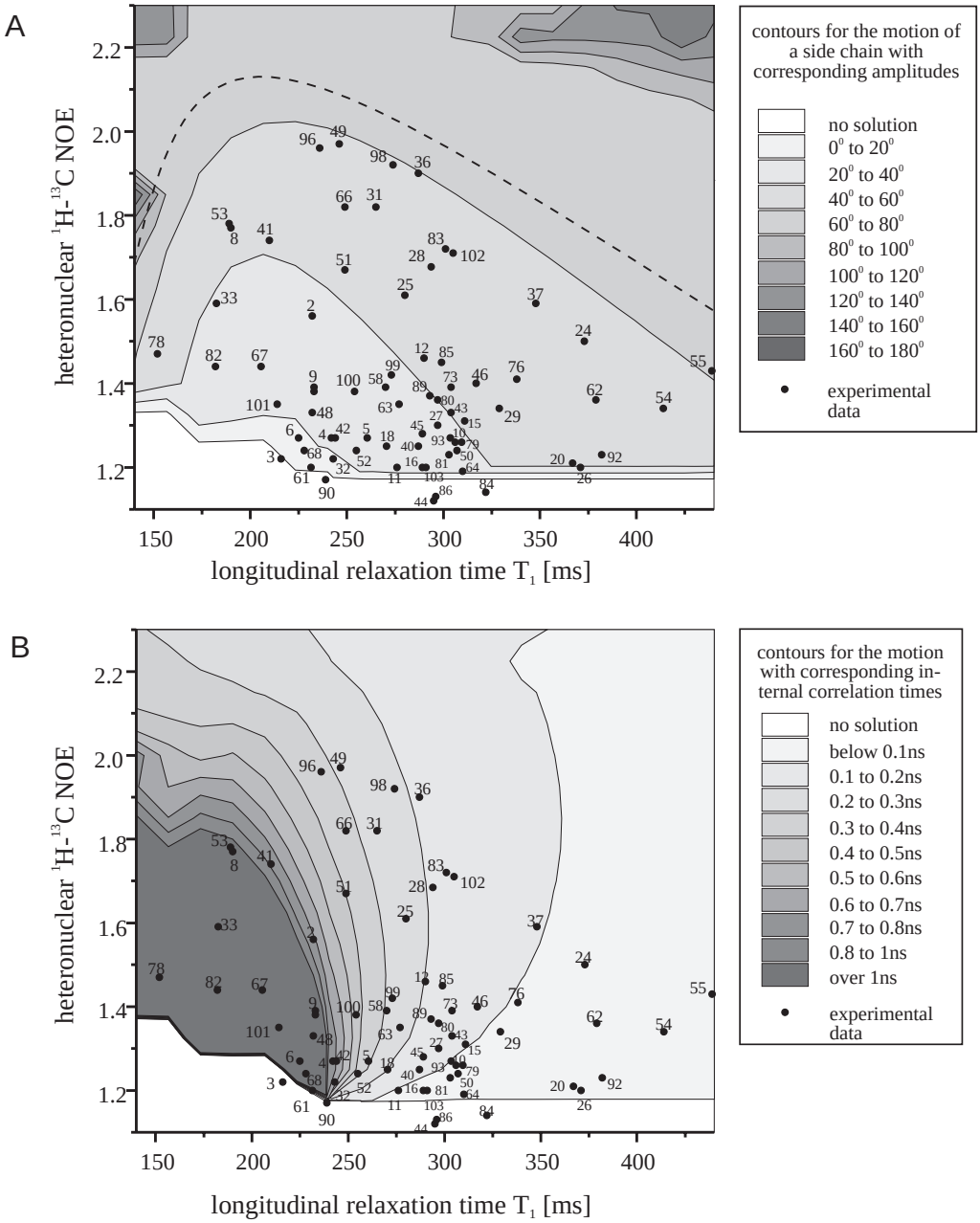

Figure 9. Contour plots of the angular amplitude (A) and the internal correlation time (B) for β-CH and β-CH_2 groups in dependence of the ^{1}H-^{13}C NOE and the longitudinal relaxation time. In the calculations, a CH_2 group was assumed to be bound to two adjacent ^{13}C nuclei. The overall correlation time τ_C was set to 4.8 ns and the ^{13}C resonance frequency to 125 MHz.

plots in Figure 9. The experimental values are also indicated in the diagrams. Only for those $^{13}C^{\beta}$ nuclei the neighbourhood of which is identical to those for which the calculation is carried out the microdynamical parameters are directly comparable. From Figure 9A it seems obvious that the increase of NOE values and the corresponding flexibility parameter are correlated. For a $^{13}C^{\beta}$ nucleus with a heteronuclear NOE value of 1.7, the angular amplitude amounts to at least 40 °. The reverse conclusion that a small NOE value is indicative of a strongly restricted motion is certainly wrong. Considering Ser^{54} as a typical example, an amplitude

of 55 ° results from a NOE value of only 1.34. From the T_1 relaxation time, upper limits for the internal correlation time can be determined. For a $^{13}C^{\beta}$ nucleus with a longitudinal relaxation time of 250 ms, the motion of the corresponding $^{13}C^{\beta}$-$^{1}H^{\beta}$ bond is faster than 400 μs in most cases. The motion of most of the β-CH and β-CH_2 groups of RNase T1 can be characterized by an angular amplitude between 0 ° and 50 ° and an internal correlation time in the range of 100–800 ps. The side chains of the residues in loop II (43–55) and loop V (93–99) show an increased flexibility with amplitudes up to 64 °. The dashed line in Figure 9 is valid for T_1-NOE combinations to which a three side jump model for the motion of the CH_2 group is applied. This type of motion may only be applicable for very few $^{13}C^{\beta}$ groups. Indeed, for these nuclei the type of motion cannot be considered. For all other nuclei with a 'large' distance from the dashed line, a three side jump model is rather improbable.

A common problem of relaxation studies refers to the selection of suitable relaxation rates to be measured. Besides the feasibility of corresponding measurements, the extent of independent information obtained from the different relaxation rates is important. Fushman et al. (1994) showed that the knowledge of only one of the ^{15}N T_1 or T_2 relaxation times may be sufficient to determine the order parameter S^2 of the N-H bond, provided the overall correlation time τ_C is known. However, both values are not sufficient for a correct calculation of the internal correlation time, since small errors in these parameters may lead to a larger uncertainty in the evaluation of the latter. The two contour plots in Figure 9 indicate that the longitudinal relaxation times and the NOEs depend on the microdynamical parameters in a clearly different manner, and therefore provide independent information. While in plot (A) (Figure 9) the contour lines are oriented rather horizontal, in plot (B) they are more vertically oriented. The advantages of using these two relaxation rates become apparent when comparing the residues Pro^{55} and Val^{78}. For both $^{13}C^{\beta}$ nuclei, a NOE value of 1.45 is observed, but they differ in their T_1 relaxation time in a pronounced manner. From the calculations it has been derived that for Pro^{55} the NOE value results from the ring-puckering process with an amplitude of 64 ° and a rapid internal correlation time of 36 ps, while for Val^{78} the same NOE value is caused by a slow reorientation of the β-CH group with a correlation time of 2.3 ns and an amplitude of 48 °.

Conclusions

It has been demonstrated that the technique of SIIS cross relaxation in combination with the measurement of the longitudinal relaxation rates is suitable to characterize the motion of side chains in proteins. In particular cases, quantitative microdynamical parameters for the motion around the χ_1 dihedral angle can be derived. The short experimental time of about 1 week and the simple analysis make this methodological approach suitable for obtaining an insight into the motions of individual amino acid side chains. Since a detailed description of side chain motion is still very difficult, it would be useful to combine information obtained from various independent experiments. Therefore, an investigation of the side chain dynamics of RNase T1 with NMR relaxation rates and ^{3}J coupling constants is currently in progress.

Acknowledgements

We thank Stefan Geschwindner and Harald Thüring for the preparation of the $^{13}C/^{15}N$-labeled protein sample, Matthias Haun and Michael Marek for computer technical support, and Dr. David Fushman (Rockefeller University, New York, NY) for making available software routines for fitting the relaxation data. We are most grateful to Stefania Pfeiffer and Yasmin Karimi-Nejad for helpful discussions. We also thank the Deutsche Forschungsgemeinschaft for a grant (Ru145/8-7). J.E. is the recipient of a stipend from the Graduiertenkolleg 'Proteinstrukturen, Dynamik und Funktion' of the University of Frankfurt.

References

Balasubramanian, S., Nirmala, R., Beveridge, D.L. and Bolton, P.H. (1994) *J. Magn. Reson.*, **B104**, 240–249.

Boyd, J., Hommel, U. and Campbell, I.D. (1990) *Chem. Phys. Lett.*, **175**, 477–482.

Bruccoleri, R.E. (1995) *J. Am. Chem. Soc..*, **117**, 10841–10854.

Buck, M., Boyd, J., Redfield, C., MacKenzie, D.A., Jeenes, D.J., Archer, D.B. and Dobson, C.M. (1995) *Biochemistry*, **34**, 4041–4055.

Bull, T.E. (1992) *Prog. NMR Spectrosc.*, **24**, 377–410.

Bystrov, V.F. (1976) *Prog. NMR Spectrosc.*, **10**, 41–81.

Clore, G.M., Driscoll, P.C., Wingfield, P.T. and Gronenborn, A.M. (1990a) *Biochemistry*, **29**, 7387–7401.

Clore, G.M., Szabo, A., Bax, A., Kay, L.E., Driscoll, P.C. and Gronenborn, A.M. (1990b) *J. Am. Chem. Soc.*, **112**, 4989–4991.

Daragan, V.A., Kloczewiak, M.A. and Mayo, K.H. (1993) *Biochemistry*, **32**, 10580–10590.

Daragan, V.A. and Mayo, K.H. (1993a) *Biochemistry*, **32**, 11488–11499.
Daragan, V.A. and Mayo, K.H. (1993b) *Chem. Phys. Lett.*, **206**, 393–400.
Daragan, V.A. and Mayo, K.H. (1996) *J. Magn. Reson.*, **B110**, 164–175.
Engelke, J. and Rüterjans, H. (1995) *J. Biomol. NMR*, **5**, 173–182.
Ernst, M.C. (1993) Dissertation ETH No. 10390, Zürich.
Ernst, M.C. and Ernst, R.R. (1994) *J. Magn. Reson.*, **A110**, 202–213.
Farrow, N.A., Zhang, O., Forman-Kay, J.D. and Kay, L.E. (1994) *J. Biomol. NMR*, **4**, 727–734.
Fushman, D., Weisemann, R., Thüring, H. and Rüterjans, H. (1994) *J. Biomol. NMR*, **4**, 61–78.
Goldman, M. (1984) *J. Magn. Reson.*, **60**, 437–452.
Grzesiek, S., Anglister, J. and Bax, A. (1993) *J. Magn. Reson.*, **B101**, 114–119.
Habazettl, J., Myers, L.C., Yuan, F., Verdine, G.L. and Wagner, G. (1996) *Biochemistry*, **35**, 9335–9348.
Hartmann, S.R. and Hahn, E.L. (1962) *Phys. Rev.*, **128**, 2042–2043.
Hartzell, C.J., Stein, P.C., Lynch, T.J., Werbelow, L.G. and Earl, W.L. (1989) *J. Am. Chem. Soc.*, **111**, 5114–5120.
Henry, G.D., Weiner, J.H. and Sykes, B.D. (1986) *Biochemistry*, **25**, 590–598.
Karimi-Nejad, Y., Schmidt, J.M., Rüterjans, H., Schwalbe, H. and Griesinger, C. (1994) *Biochemistry*, **33**, 5481–5492.
Karplus, M. (1959) *J. Chem. Phys.*, **30**, 11–13.
Karplus, M. (1963) *J. Am. Chem. Soc..*, **85**, 2870–2871.
Kay, L.E., Torchia, D.A. and Bax, A. (1989) *Biochemistry*, **28**, 8972–8979.
Kay, L.E., Nicholson, L.K., Delaglio, F., Bax, A. and Torchia, D.A. (1992) *J. Magn. Reson.*, **97**, 359–375.
Lipari, G. and Szabo, A. (1980) *J. Biophys.*, **30**, 489–506.
Lipari, G. and Szabo, A. (1981) *J. Chem. Phys.*, **75**, 2971–2976.
Lipari, G. and Szabo, A. (1982a) *J. Am. Chem. Soc.*, **104**, 4546–4559.
Lipari, G. and Szabo, A. (1982b) *J. Am. Chem. Soc.*, **104**, 4559–4570.
Loh, S.N., Prehoda, K.E., Wang, J. and Markley, J.L. (1993) *Biochemistry*, **32**, 11022–11028.
London, R.E. and Avitabile, J. (1978) *J. Am. Chem. Soc.*, **100**, 7159–7165.
London, R.E. (1980) In *Magnetic Resonance in Biology* (Ed., Cohen, J.S.) Vol. 1, Wiley, New York, NY, pp. 1–69.
Mádi, Z.L., Griesinger, C. and Ernst, R.R. (1990) *J. Am. Chem. Soc.*, **112**, 2908–2914.
Martinez-Oyanedel, J., Choe, H., Heinemann, U. and Saenger, W. (1991) J. Mol. Biol., **222**, 335–352.
Mohebbi, A. and Shaka, A.J. (1991) *Chem. Phys. Lett.*, **178**, 374–378.
Nicholson, L.K., Kay, L.E., Baldisseri, D.M., Arango, J., Young, P.E., Bax, A. and Torchia, D.A. (1992) *Biochemistry*, **31**, 5253–5263.
Nirmala, N.R. and Wagner, G. (1988) *J. Am. Chem. Soc.*, **110**, 7557–7558.
Palmer III, A.G., Rance, M. and Wright, P.E. (1991) *J. Am. Chem. Soc.*, **113**, 4371–4380.
Palmer III, A.G. and Case, D.A. (1992) *J. Am. Chem. Soc.*, **114**, 9059–9067.
Palmer III, A.G., Hochstrasser, R.A., Millar, D.P., Rance, M. and Wright, P.E. (1993) *J. Am. Chem. Soc.*, **115**, 6333–6345.
Richarz, R., Nagayama, K. and Wüthrich, K. (1980) *Biochemistry*, **19**, 5189–5196.
Schmidt, J.M., Brüschweiler, R., Ernst, R.R., Dunbrack, R.L., Joseph, D. and Karplus, M. (1993) *J. Am. Chem. Soc.*, **115**, 8747–8756.
Sklenář, V., Torchia, D. and Bax, A. (1987) *J. Magn. Reson.*, **73**, 375–379.
Smith, L.J., Mark, A.E., Dobson, C.M. and van Gunsteren, W.F. (1995) *Biochemistry*, **34**, 10918–10931.
Stone, M.J., Fairbrother, W.J., Palmer III, A.G., Reizer, J., Saier, M.H. and Wright, P.E. (1992) *Biochemistry*, **31**, 4394–4406.
Szyperski, T., Luginbühl, P., Otting, G., Güntert, P. and Wüthrich, K. (1993) *J. Biomol. NMR*, **3**, 151–164.
Wittebort, R.J. and Szabo, A. (1978) *J. Chem. Phys.*, **69**, 1722–1736.
Yamazaki, T., Muhandiram, R. and Kay, L.E. (1994) *J. Am. Chem. Soc.*, **116**, 8266–8278.
Ye, C., Fu, R., Hu, J., Hou, L. and Ding, S. (1993) *Magn. Reson. Chem.*, **31**, 699–704.
Zhu, L., Kemple, M.D., Landy, S.B. and Buckley, P. (1995) *J. Magn. Reson.*, **109**, 19–30.